International Journal of Greenhouse Gas Control 29 (2014) 248–255

Contents lists available at ScienceDirect

International Journal of Greenhouse Gas Control

journal homepage: www.elsevier.com/locate/ijggc

CO_2 saturation and thickness predictions in the Tubåen Fm., Snøhvit field, from analytical solution and time-lapse seismic data

S. Grude[a,*], M. Landrø[a,1], J.C. White[b,2], O. Torsæter[a,3]

[a] NTNU, S.P. Andersens vei 15A, 7491 Trondheim, Norway
[b] British Geological Survey, Keyworth, Nottingham NG12 5GG, UK

ARTICLE INFO

Article history:
Received 2 June 2014
Received in revised form 13 August 2014
Accepted 15 August 2014

Keywords:
The Snøhvit field
CO_2 storage
Time-lapse seismic
CO_2 saturation
CO_2 layer thickness

ABSTRACT

CO_2 migration in a saline aquifer is governed by viscous, capillary and gravitational fluid forces at an early stage of injection, where the dominant flow regime is site specific and controls the fluid migration in the pore space. This study combines the CO_2 saturation inverted from time-lapse seismic methods with an analytical expression to define the CO_2 flow regime, saturation distribution and layer thickness in the Tubåen Fm. following CO_2 injection. Quantitative estimates of the CO_2 saturation from time-lapse seismic amplitude versus offset (AVO) and spectral decomposition are compared to a viscous dominated analytical expression of CO_2 injection into a saline aquifer. The spatial extent of the CO_2 plume obtained from time-lapse spectral decomposition and inverted from time-lapse AVO analysis display good agreement with the analytical expression. The CO_2 is limited to an area close to the injection well, with an elongated shape in the channel direction. Comparison between the time-lapse seismic and analytical expression shows that the fluid flow is dominated by viscous forces. CO_2 saturation within the plume is constant and close to the residual brine saturation. The influence of gravity is ignorable on the reservoir CO_2 flow. CO_2 fills the entire sandstone unit up to approximately 50 m away from the injection before the CO_2 layer thickness is reduced to a thin wedge that propagates below the overlying shale unit. Reduction in CO_2 saturation away from the injection well is a reduction in effective CO_2 saturation relative to the thickness of the horizon. The maximum radius of the CO_2 layer from the analytic expression is 750 m, of which 400 m is above the time-lapse noise level. Time-lapse seismic analysis reveals the CO_2 layer radius is 405 m in the direction of the local fluvial channel and 273 m in the perpendicular direction.
© 2014 Elsevier Ltd. All rights reserved.

1. Introduction

CO_2 migration in a saline aquifer is governed by viscous, capillary and gravitational fluid forces at an early stage of injection (Lindeberg and Wessel-Berg, 1997). The dominant flow regime is site specific and depends among others on injection rate, aquifer volume, reservoir injectivity, reservoir depth, formation pressure and temperature. CO_2 must overcome the capillary entry pressure to migrate into brine-saturated pores (Bryant et al., 2008). Viscous force is pressure driven and is dependent on the injection overpressure (Class et al., 2009). Supercritical CO_2 is less dense and less viscous than the resident formation brine. The mobility contrast between supercritical CO_2 and brine, combined with the effect of gravity will lead to vertical segregation of the fluids, and a thin layer of CO_2 will be formed at the top of the formation (Nordbotten et al., 2005).

CO_2 migration in a saline aquifer has been studied widely through analytical models, simulations and laboratory experiments. Nordbotten and Celia (2006) described viscous dominated CO_2 migration from an analytical expression, whilst Taku et al. (2007) performed flow modelling simulations to investigate the interplay between viscous forces, gravity forces and capillary trapping of CO_2. Møll Nilsen et al. (2011) simulated long term CO_2 storage in the Sleipner Fm. based on vertical equilibrium (VE) and Polak et al. (2011) investigated the influence of gravitational, viscous and capillary effects on the vertical flow of CO_2 from experimental studies. Cavanagh (2013) found that a gravity-segregated/capillary-dominated model best described the CO_2 layer at a relatively short distance from the injection well at the Sleipner CO_2 injection site.

* Corresponding author. Tel.: +47 73 59 11 40.
E-mail addresses: sissel.grude@ntnu.no (S. Grude), martin.landro@ntnu.no (M. Landrø), jame3@bgs.ac.uk (J.C. White), ole.torsater@ntnu.no (O. Torsæter).
[1] Tel.: +47 73 59 49 73.
[2] Tel.: +44 0115 936 3354.
[3] Tel.: +47 73 59 49 41.

http://dx.doi.org/10.1016/j.ijggc.2014.08.011
1750-5836/© 2014 Elsevier Ltd. All rights reserved.

The main purpose of monitoring the injected CO_2 is to demonstrate safe storage and detect possible leakage. Monitoring will also give valuable information regarding CO_2 migration and highlight the dominant flow regime inside the storage reservoir. Several reservoir parameters may change due to CO_2 injection. Changes in fluid saturation and pore pressure, and geomechanical changes in the reservoir, are most frequently observed. Time-lapse seismic methods are used to monitor CO_2 injected in saline aquifers, and give a good understanding of the plume migration and CO_2 saturation (Arts et al., 2004; Chadwick et al., 2006; Osdal et al., 2013). Numerous studies have quantified the CO_2 injected at the Sleipner field. Chadwick et al. (2010) summarizes these studies, which have included amplitude-thickness tuning relationships, stratigraphic inversion, reflection amplitude analysis and topographic analysis. Williams and Chadwick (2012) used spectral decomposition to assess the thickness and velocities of thin layers at Sleipner. Ivanova et al. (2012) used petrophysical and pulsed neutron-gamma logging measurements to quantify the amount of CO_2 visible in the time-lapse seismic data at the Ketzin field. Nakatsuka et al. (2009) estimated CO_2 saturation from resistivity, and emphasized that the approach is valuable for CO_2 saturation above a certain threshold, where the seismic methods lack resolution. Osdal et al. (2013) predicted CO_2 saturation and thickness in the Stø Fm. at the Snøhvit field by comparing synthetic seismic and time-lapse seismic.

Approximately 0.5 Mt of CO_2 was injected into the Tubåen Fm. at the Snøhvit field between April 2008 and September 2009. Injection was associated with a pressure build-up, and following a well intervention operation the Stø Fm. was used for further CO_2 injection, avoiding the pressure limitations in the Tubåen Fm. (Hansen et al., 2013). Time-lapse amplitude versus offset (AVO) inversion (Grude et al., 2013) and spectral decomposition (White et al., 2014) were used to separate the pressure and fluid effects on the time-lapse seismic data. This study develops a better understanding of CO_2 saturation and layer thickness in the Tubåen Fm. by combining the saturation inverted from time-lapse seismic methods and a viscous dominated analytical expression of CO_2 plume thickness (Nordbotten and Celia, 2006).

2. Tubåen Fm., the Snøhvit field

The Tubåen Fm. is located at 2560-2670 m depth (TVD) below the sea surface. The CO_2 storage reservoir is approximately 2500 m wide close to the injection well, compartmented by sealing faults in east–west direction.

The depositional environment is predominately deltaic, with marine and tidal influence (Hansen et al., 2013). The formation can be subdivided into four sandstone units, Tubåen 1-4, separated by interbedded shale units, as seen from the GR in Fig. 1. CO_2 was injected through three perforations covering the lowermost Tubåen 1-3 sandstone units, highlighted by the grey vertical lines alongside the GR log. Approximately 80% of the CO_2 has migrated into the Tubåen 1 sandstone unit, whereas the remaining 20% has migrated into the Tubåen 2 and 3 units (Hansen et al., 2011). The Tubåen 1 unit is interpreted to be sandstone channel trending in a north–south direction. Analysis of pressure data and time-lapse seismic data indicate that the shale unit above Tubåen 1 limits vertical migration of the CO_2 (Eiken et al., 2011; Hansen et al., 2011). Grude et al. (2014) came to the same conclusion by comparing time-lapse and synthetic seismic data.

Tubåen 1 sandstone channels are approximately 10-15 m thick and reach to the sealing faults. Average permeability is 750 mD and porosity 0.19. A summary of the reservoir properties in Tubåen 1 can be seen in Table 1. The injected CO_2 is dried down to <50 ppm water content and a 0.5-2% methane fraction is present (Eiken et al., 2011). CO_2 and brine fluid properties estimated at the reservoir pressure of 290 bar, temperature of 95 °C and brine salinity of 14% are given in Table 2.

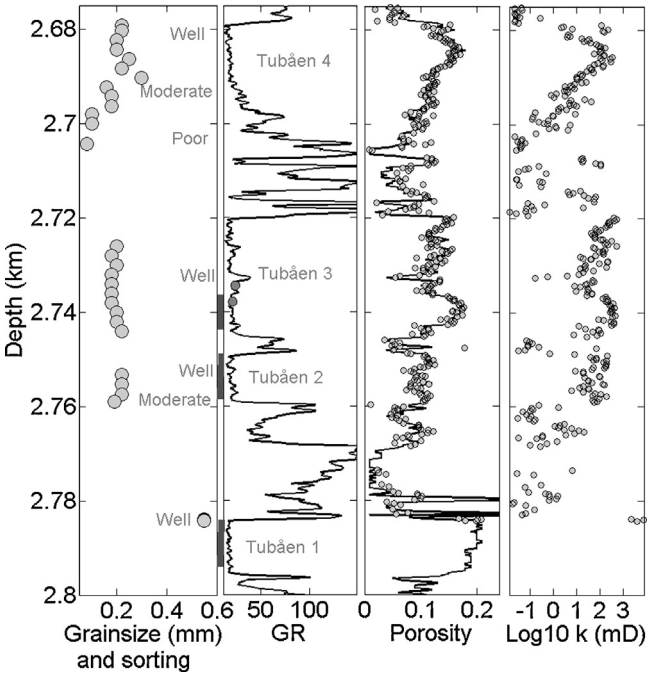

Fig. 1. Depth plots from the injection well. Left to right: grain size and sorting determined from thin sections, gamma ray (GR), porosity and permeability measured in laboratory. The vertical axis shows measured depth in km, the well is slightly deviated. The reservoir zone is located between 2.68 and 2.8 km. The four Tubåen sandstone units can be seen in the gamma log, separated by shale units. The perforated intervals are marked with grey vertical lines on the GR. The grey circles overlain on the GR show the locations of the core samples.

Table 1
Average reservoir properties, mobility ratio and gravity factor for the Tubåen 1 sandstone unit.

Thickness	h	14	m
Porosity	φ	0.19	Fraction
Permeability	k	750	mD
Residual brine saturation	S_{br}	0.13[a]	Fraction
Relative permeability of CO_2 at S_{br}	k_{r,CO_2}	0.7[b]	Fraction
Injected volume	Q (ktons/s) × t (s)	400	ktons
Mobility ratio	$\lambda(\lambda_{CO_2}/\lambda_{Brine})$	5.65	
Gravity factor	Γ	0.6	

[a] Estimated from (Sengupta, 2000), taking the porosity and permeability into consideration.

[b] No laboratory measurement available from Tubåen 1. The value is assumed from comparison with laboratory measurements of the relative permeability on three composite cores from the Tubåen 3 sandstone unit at 2735 m measured depth (MD) and published literature (Bennion and Bachu, 2008).

Table 2
Fluid properties estimated at reservoir pressure of 290 bar, temperature of 95 °C and brine salinity of 14%. The CO_2 density is estimated from the (Span and Wagner, 1996) equation of state. CO_2 viscosity is estimated from (Scalabrin et al., 2006). Brine density is estimated from (Batzle and Wang, 1992). Brine viscosity is estimated from (Kestin et al., 1978).

CO_2 density	ρ_{CO_2}	663	kg/m^3
Brine density	ρ_{Brine}	1090	kg/m^3
CO_2 viscosity	μ_{CO_2}	0.055	mPa s
Brine viscosity	μ_{Brine}	0.444	mPa s

In this study, 3D seismic surveys undertaken in 2003 and 2009 are utilized and repeatability metrics between the vintages are high (Hansen et al., 2013). The surveys cover a common lateral extent of approximately 8 × 9.5 km. Fig. 2 displays a cross-section, which intersects the well location, from the baseline seismic survey (lower

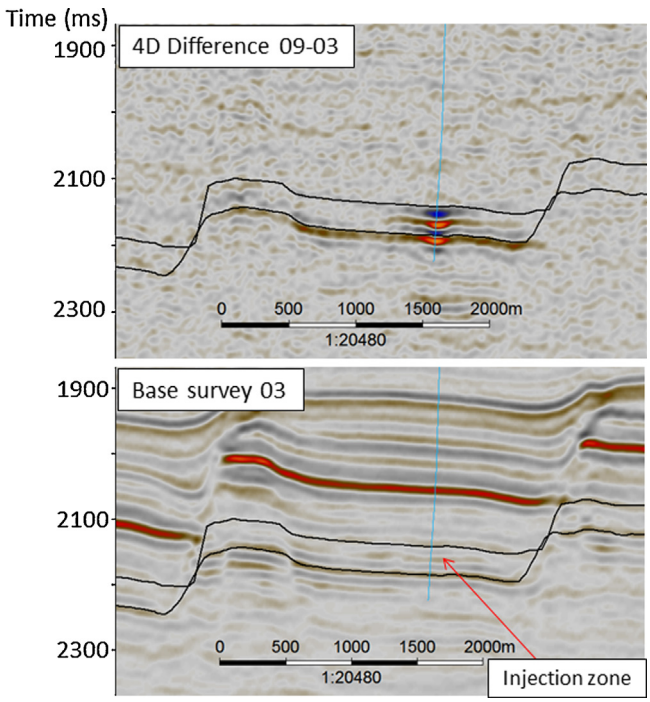

Fig. 2. Cross-section through the reservoir zone. The uppermost picture shows time-lapse difference between the seismic surveys. The lowermost picture is from the 2003 survey. The top and base of the reservoir zone are shown by the black lines and the injection well is the blue vertical line. The injection zone is marked by the red arrow. (For interpretation of the references to colour in this figure legend, the reader is referred to the web version of this article.)

Source: figure from Grude et al. (2013).

panel) and the same section from the time-lapse seismic difference data (upper). The response generated as a consequence of injection is clear.

As such, this study focuses on the 400 ktons of CO_2 injected into the Tubåen 1 sandstone unit prior to the first monitoring survey in September 2009.

3. CO_2 layer thickness and saturation estimated from the analytical expression

Capillary pressure measured on two core plugs from the Tubåen 3 sandstone unit can be seen in Fig. 3. Porosity and permeability measurements from the core plugs are inset in the figure. The location of the core plugs is shown with grey circles in the GR log in Fig. 1. The capillary entry pressure is 0.1 bar and the capillary

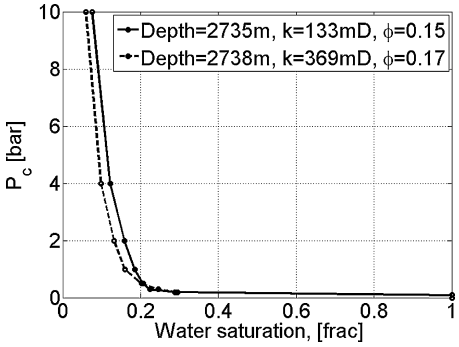

Fig. 3. Laboratory measurements of capillary pressure on 2 core plug from the Tubåen 3 sandstone unit (courtesy Statoil). Depth, porosity and permeability are given in the figure legend. The location of the samples is shown by the grey circles in the GR in Fig. 1.

pressure is 1 MPa at residual brine saturation obtained in the laboratory for these samples. The capillary pressure is low compared to the injection overpressure of maximum 6-10 MPa. No measurement of capillary pressure was performed on core plugs from the Tubåen 1 sandstone unit, but the capillary pressure is most likely negligible based on the measurements in Tubåen 3 and the average permeability of 750 mD in Tubåen 1. Laboratory measurements of the vertical and horizontal permeability were performed on core plugs from the sandstone units. These showed that the permeability was approximately similar in both directions. Gravitational forces are expected to be small in this 10-15 m thick sandstone unit with vertical permeability of 750 mD. It is reasonable to assume that viscous forces govern the CO_2 flow in the Tubåen 1 sandstone unit.

Nordbotten et al. (2005) and Nordbotten and Celia (2006) developed an analytical expression which describes the shape of a CO_2 plume when the capillary pressure is neglected. In this model, the CO_2 is injected into a porous formation that is confined above and below by impermeable cap rock formations. The expression is viscous dominated, with influence from gravity. Their dimensionless gravity factor, Γ, can be used to identify when the gravity force contributes to the fluid flow (Eq. (14) in Nordbotten et al. (2005)):

$$\Gamma = \frac{2\pi\Delta\rho g\lambda_b kB^2}{Q_{well}} \quad (1)$$

$\Delta\rho = \rho_{Brine} - \rho_{CO_2}$ is the difference in density between brine and CO_2, g is the gravitational constant, $\lambda_b = k_{r,b}/\mu_b$ is the mobility of brine in the formation, which depends on the relative permeability and viscosity of the brine. The saturation in the brine phase is 1 due to the assumptions of immiscible fluids, this makes $k_{r,b} = 1$ (Okwen et al., 2010). B is the thickness of the formation, k is the vertical permeability and Q_{well} is the injection rate (Nordbotten et al., 2005). Nordbotten et al. (2005) and Nordbotten and Celia (2006) found that a lower cut-off value of 1, for the gravity factor, is suitable to illustrate when gravity forces exert an influence on the CO_2 flow. Okwen et al. (2010) revised the cut-off value to 0.5, to within 10% error. Based on this equation one observed that the influence of gravity increases with the thickness of the formation and vertical permeability, and decreases with increasing brine viscosity and injection rate. The gravity factor is estimated to be approximately 0.6, using Eq. (1), in the Tubåen 1 sandstone unit. This value is at the lower cut-off for gravity influenced flow and it is reasonable to neglect this effect as CO_2 migration is expected to be viscous dominated.

Supercritical CO_2 is less dense and less viscous than the formation brine therefore injected CO_2 will migrate upwards and along the overlying shale due to the density difference, which affects both the gravity segregation and mobility ratio ($\lambda_{CO_2}/\lambda_{Brine}$, where λ_{CO_2} and λ_{Brine} are the mobilities of the CO_2 and brine respectively) (Nordbotten and Celia, 2006). This will lead to a low saturation of CO_2 inside the formation. The mobility ratio between CO_2 and brine is defined as:

$$\frac{\lambda_{CO_2}}{\lambda_{Brine}} = \frac{k_{r,CO_2}}{k_{r,Brine}}\frac{\mu_{Brine}}{\mu_{CO_2}} \quad (2)$$

Using estimates of the relative permeability and viscosities of the two fluids, Table 2, a mobility ratio of 5.65 is derived in the Tubåen Fm. This mobility ratio is strongly dependent on the viscosity for the Tubåen 1 sandstone unit, as the CO_2 has a much lower viscosity than the formation brine at the reservoir pressure of 290 bar, temperature of 95 °C and brine salinity of 14%. A mobility ratio of 5.65 is relative low compared to typical mobility ratios of 5-20 for CO_2 displacing brine (Okwen et al., 2010). Table 1 summarizes the reservoir parameters of the Tubåen 1 unit, including the estimated mobility ratio and gravity factor.

The thickness and effective saturation of the CO_2 layer obtained from the analytical expression can be found in Fig. 4. The sandstone

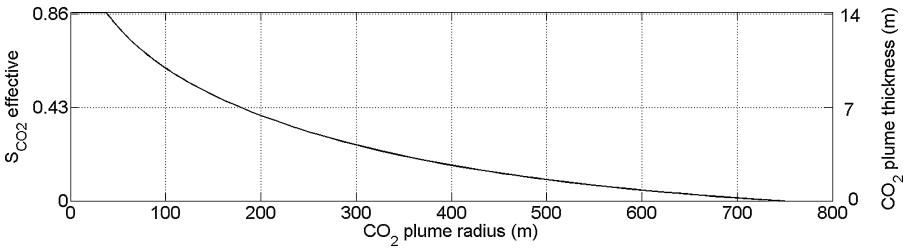

Fig. 4. Analytical expressions for the effective CO_2 saturation and CO_2 plume thickness based on Nordbotten and Celia (2006). The input parameters for the analytical solution are given in Tables 1 and 2. The maximum CO_2 saturation corresponds to 0.87 (1-residual brine saturation).

unit is filled with CO_2 to approximately 40 m from the injection well, before the CO_2 layer thins due to vertical segregation. The maximum radius of the CO_2 layer is approximately 750 m. The CO_2 saturation within the plume is uniformly distributed, and equal to 1-residual brine saturation, which is estimated to $S_{br} = 0.13$ for the Tubåen 1 sandstone unit. The effective CO_2 saturation of the Tubåen 1 sandstone unit decreases linearly with the CO_2 layer thickness.

4. CO_2 layer thickness and saturation from time-lapse seismic data

The time-lapse seismic signature from the Tubåen Fm. is influenced by both pore pressure and saturation changes. Two methods have been applied to separate these effects (Grude et al., 2013; White et al., 2014). Both methods focus on the lowermost Tubåen 1 sandstone unit where 80% of the injected CO_2 migrated.

White et al. (2014) utilized spectral decomposition (Laughlin et al., 2002) to separate the pore pressure and saturation induced time-lapse seismic signatures. Their results are based on the assumption that the saturation anomaly created by the injected CO_2 in the sandstone units will migrate as a thinner layer than the pore pressure response, which will spread more widely through the reservoir. These different vertical extents will tune different frequencies in the seismic wavelet. White et al. (2014) used a 25 Hz spectral cut-off to discriminate the region dominated by increased pore pressure. Conversely, changes above 30 Hz are most likely due to fluid substitution. Spectral decomposition separates the pore pressure and saturation effects on the time-lapse seismic data, but does not give any quantitative estimates of pressure and saturation changes. Pore pressure communication between the Tubåen sandstone units is needed to explain the vertical extent of the pore pressure anomaly. Capillary pressure limits vertical CO_2 migration between the Tubåen 1 and 2 sandstone units.

Grude et al. (2013) inverted for injection related pore pressure and saturation changes from near and far stack time-lapse seismic. The inversion algorithm was introduced by Landrø (2001) and uses rock physics to relate the seismic parameters to pressure and saturation. The relationship between the seismic response and the saturation depends on the CO_2 distribution in the pore space. Patchy (Voigt, 1887) and uniform (Reuss, 1929) fluid mixing models represent the upper and lower bounds for the fluid distribution. (Grude et al., 2013) compared the CO_2 saturation obtained from the upper and lower bounds with the CO_2 saturation derived using an intermediate CO_2 distribution, represented by the Brie equation with an exponent $e = 3$ in the inversion. The Brie's equation of fluid moduli reads $K_f = (K_{Brine} - K_{CO_2})S_{Brine}^3 + K_{CO_2}$ (Brie et al., 1995). The different CO_2 distributions gave the same spatial extent of the saturation anomaly, with the difference being the magnitude of the CO_2 saturation. The intermediate CO_2 distribution was found to be most likely from comparison of time-shift from cross-correlation and time-shift estimated from the inverted pressure and saturation. The intermediate CO_2 distribution gave a maximum CO_2 saturation of 0.22 close to the well. A straight-line approximation was found

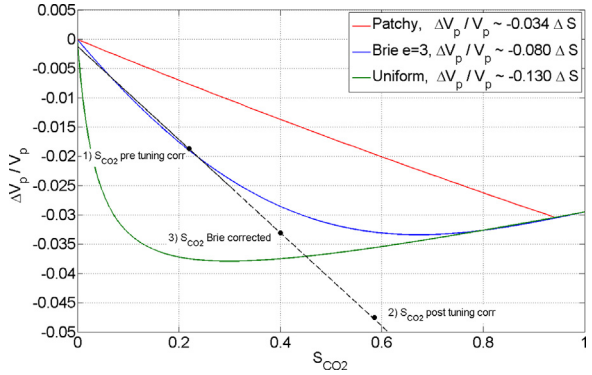

Fig. 5. Relative change in P-wave velocity from fluid substitution with CO_2 replacing brine in Gassmann's equation (Gassmann, 1951). CO_2 saturation according to a patchy CO_2 distribution (red), uniform CO_2 distribution (green) and an intermediate distribution (blue) explained by Brie's equation (Brie et al., 1995). The black line shows a linear approximation to the intermediate CO_2 distribution. The linear approximation is valid up to $S_{CO_2} \sim 0.3$, and dashed interpolation is shown after that point. The black dots illustrate the CO_2 saturation before tuning correction (1), after tuning correction (2), and corrected for the error introduced by the straight-line approximation (3). (For interpretation of the references to colour in this figure legend, the reader is referred to the web version of this article.)
Source: figure modified from Grude et al. (2013).

to the velocity-saturation curve. The straight-line approximation introduced an error of 5% at $S_{CO_2} = 0.3$ with a CO_2 distribution according to Brie's equation (Fig. 5). The velocity-saturation curve becomes highly non-linear after approximately $S_{CO_2} = 0.3$ and this value was used as a threshold for when the inversion was valid. CO_2 saturations above ~0.3-0.4 follow another trend where the slope is almost flat, and it is difficult to differentiate saturations from rock physics.

Results from spectral decomposition show that the inverted CO_2 saturation should be regarded as a new, or significantly altered, thin subsurface layer. Juhlin and Young (1993) found that thin layers imbedded in a homogeneous rock can significantly affect the AVO response compared to that of a simple interface of the same lithology. A correction for offset-dependent tuning should therefore be applied to the saturation response to get the true reflectivity, this correction was not performed in Grude et al. (2013). Widess (1973) found a correlation between layer thickness and reflection amplitude then Lin and Phair (1993) extended this work to include offset dependence, here expressed in terms of changes in reflectivity:

$$\Delta R(\theta)_{Tuned} = f_0 \Delta T \cos(\theta) \Delta R(\theta) \quad (3)$$

The equation applies for layers with thickness below $\lambda/4$ (Widess, 1973), and assumes a thin layer interbedded in a homogeneous rock. f_0 is the dominant frequency of the wavelet (here equal to 40 Hz) and ΔT *is* the two way travel time at normal incidence (~0.013 s in the Tubåen 1 sandstone unit). $R(\theta)$ is the true reflectivity. The average reflection angle, θ, in the near stack is 8° (1-17°)

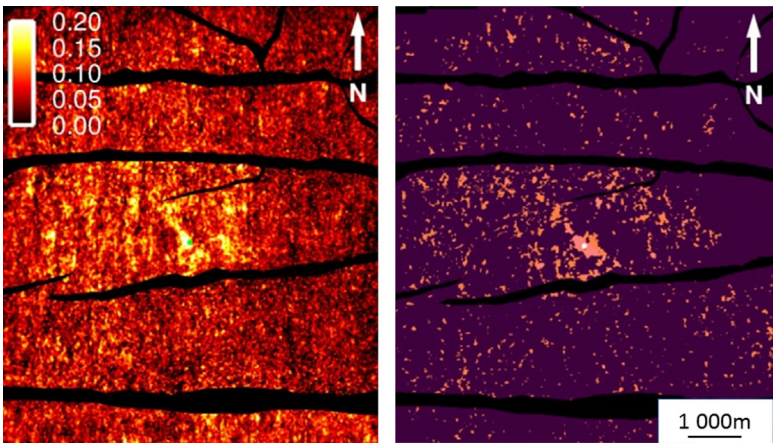

Fig. 6. Left: CO_2 saturation inverted from time-lapse AVO seismic data (Grude et al., 2013). Right: CO_2 saturation changes from spectral decomposition (White et al., 2014). The location of the injection well is marked by a circle. North direction is indicated by the arrow. The CO_2 saturation inverted from time-lapse AVO seismic data before thin layer tuning is indicated by the colour scale. No quantitative estimates of the saturation are obtained from spectral decomposition.

whilst in the far stack is 43° (34-51°). By inserting the values into Eq. (1), one obtains:

$$\Delta R_N = 1.92\Delta R_{\text{Tuned},N} \quad (4)$$

$$\Delta R_F = 2.63\Delta R_{\text{Tuned},F} \quad (5)$$

As such, the near stack should be scaled using Eq. (4), and the far stack with Eq. (5) to obtain the true reflectivity of the inverted saturation. The scaling factor was implemented in the saturation expression to get the true reflectivity. The maximum CO_2 saturation obtained after tuning correction is 0.59, which clearly violates the assumption behind the inversion of $S_{CO_2\ \text{maximum}} = 0.3$, as seen by the dashed line and point 2 in Fig. 5. The CO_2 saturation becomes approximately 0.40 after correcting for the straight-line approximation as illustrated by point 3 in the figure. $S_{CO_2} = 0.4$ is still above the validity of the straight line and no unique CO_2 saturation can be found between 0.40 and 0.87 (1-residual brine saturation). The lack of a unique solution gives the possibility of much higher saturations than originally found in Grude et al. (2013). The velocity and frequency content of the seismic data gives a maximum thin layer tuning at about 20-40 m thickness in the Tubåen Fm. (Hansen et al., 2011). The thickness of the CO_2 plume can be extracted from the effective saturation since the new subsurface layer is at maximum similar to the thickness of the sandstone unit of 14 m, which is below the tuning thickness.

The CO_2 layer distribution inverted from time-lapse AVO and spectral decomposition has an elliptical shape around the injection well in SE-NW direction (Fig. 6). A maximum radius of the CO_2 layer of 470 m is observed in the channel direction from spectral decomposition. The maximum radius inverted from time-lapse AVO is 340 m in the channel direction. CO_2 layer radius is approximately 280 m perpendicular to the channel direction inverted from time-lapse AVO seismic data, and 266 m from spectral decomposition.

5. Comparing CO_2 layer thickness and saturation from analytical solution and time-lapse seismic data

CO_2 saturation within the plume is assumed constant for both the analytical expression and in the saturation inverted from time-lapse seismic. Yet no numerical estimate is found between $S_{CO_2} = 0.4 - 0.87$ from the seismic. The analytical expression assumes a uniform CO_2 distribution in the pore space. The saturation inverted from time-lapse seismic data has a CO_2 mixing model that falls between the uniform and patchy bounds, described by the Brie's equation (Fig. 5). The difference between the velocity changes following injection for the uniform and Brie CO_2 distribution models

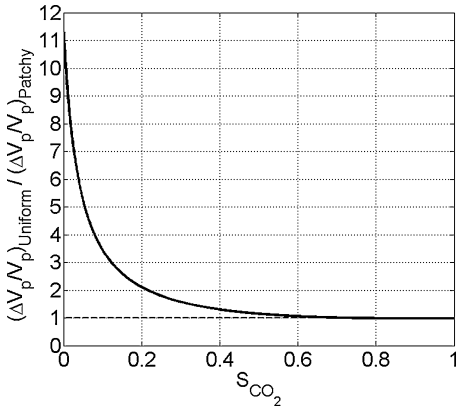

Fig. 7. Relative variation in velocity between uniform and Brie fluid distribution in the pore space. The contrast in velocity difference is large at low CO_2 saturation but ignorable above $S_{CO_2} \sim 0.5$.

are large for small amounts of CO_2, but ignorable at CO_2 saturations above approximately 0.5, as demonstrated in Fig. 7. Comparing velocity changes at a CO_2 saturation of 0.4 introduces an error of 24% between the uniform and Brie CO_2 distribution models.

The comparison of the CO_2 layer thickness and effective CO_2 saturation obtained from the analytical expression and time-lapse seismic data can be made by assuming that the saturation obtained from the analytical expression is true, and scale the S_{CO_2} from the time-lapse seismic according to this. Comparison of the shape of the layer with distance from the injection well can then indicate if the assumption of viscous dominated flow is valid, and if the CO_2 saturation within the layer is close to the residual brine saturation, as assumed in the analytical expression. Effective CO_2 saturation and layer thickness inverted from time-lapse seismic AVO can be seen in a plan view in Fig. 8 after scaling. A preferred CO_2 migration is observed in the channel direction (NW). CO_2 layer thickness is shown in the left panel of Fig. 8. The sandstone channels create an irregular fluid front. The radius of the CO_2 layer estimated from spectral decomposition, AVO and the analytical expression is summarized in Table 3.

Comparison of the CO_2 layer thickness and effective saturation from the analytical expression and the time-lapse seismic can be seen in Fig. 9. Four cross-sections are chosen for comparison, two in the channel direction (grey and red) and two perpendiculars to the channel direction (blue and green). Location of the seismic line is indicated in the figure. Background RMS seismic amplitudes

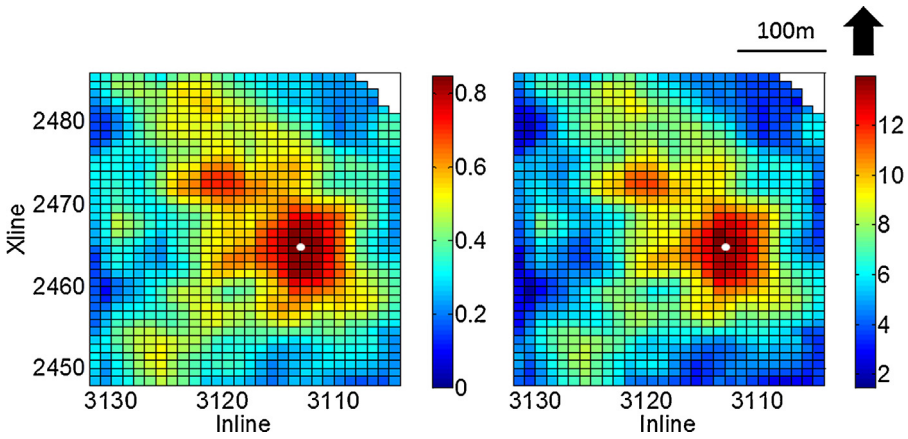

Fig. 8. Left: effective CO_2 saturation inverted from time-lapse AVO seismic data with a CO_2 distribution in the pore space from Brie's equation, scaled according to the analytical expression. Right: CO_2 layer thickness (m) derived from the effective CO_2 saturation, assuming a linear relationship. North direction is indicated by the arrow. The location of the injection well is marked in white.

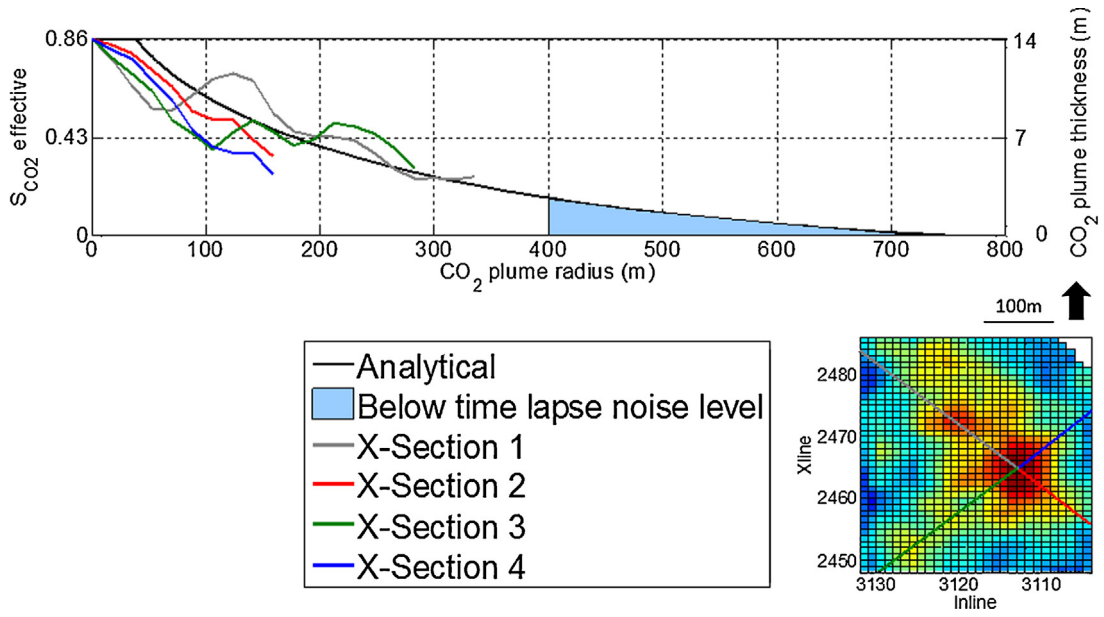

Fig. 9. Effective CO_2 saturation and CO_2 plume thickness from the analytical solution (black) and four time-lapse seismic lines (blue, green, grey and red). The time-lapse noise level is marked in the figure. The location of the seismic cross-sections is shown in the figure below. North direction is indicated by the arrow. (For interpretation of the references to colour in this figure legend, the reader is referred to the web version of this article.)

Table 3
CO_2 layer radius obtained from the analytical estimate, inverted from time-lapse AVO and spectral decomposition.

	Radius (m)
Analytical solution	400
Time-lapse AVO	340[a], 280[b]
Time-lapse spectral decomposition	470[a], 266[b]

[a] In channel direction (SE–NW).
[b] Perpendicular to channel direction (NE–SW).

measured above the Tubåen Fm. correspond to approximately 18% of the maximum saturation. This relates to $S_{CO_2\,\text{effective}} = 0.16$ on the analytical expression. As such, a CO_2 layer radius above 400 m is not detectable in the seismic data, this area is shaded in blue in Fig. 9. The decrease in CO_2 layer thickness and effective saturation inverted from time-lapse seismic follow the same trend as the analytical solution with distance from the well, but decrease more rapidly with distance from the injection well. There are many uncertainties in the input parameters that can explain the deviation. For instance, the mobility ratio is strongly dependent on relative permeability. A lower relative permeability would lead to a lower mobility ratio, and a more piston-like displacement of the fluid front. The CO_2 saturation in NW and SW direction can better describe the radius of the CO_2 plume than in the SE and NE direction. The CO_2 plume obtained from spectral decomposition are more cylindrical in shape around the well, and can better describe the plume obtained from the analytical expression. It is likely to assume that the CO_2 saturation is close to the residual brine saturation, and constant within the plume from comparison between the analytical expression and the AVO inverted seismic data.

6. Discussion

The analysis is limited to early injection times, when the primary trapping mechanisms for CO_2 are stratigraphic and structural trapping. CO_2 dissolution into the formation brine, evaporation of brine into the dry CO_2, capillary trapping and mineral trapping mechanisms are expected to dominate at a later stage

(Bachu et al., 2007; IPCC, 2005). The evaporation of the residual brine leads to formation and propagation of a drying front behind the main CO_2 invasion front where no brine is present (Nordbotten and Celia, 2006). The fraction of CO_2 dissolution into formation brine and brine evaporation into the dry CO_2 is expected to be small at early stage of injection (Nordbotten and Celia, 2006).

Laboratory measurements of capillary pressure on core samples from the Tubåen 3 sandstone unit indicate that capillary pressure can be ignored. These are samples taken at one location in a heterogeneous reservoir. Local heterogeneity may introduce capillary barriers that cannot be ignored and will influence the reservoir fluid flow. The derivation of the analytical solution makes numerous assumptions and simplifications, but concedes that they are not particularly restrictive and are approximately valid for most plausible injection scenarios. In this study, a radial CO_2 distribution around the injection well has been assumed. The assumption is clearly wrong in this fluvial environment, where an elliptical shape better describes the CO_2 layer distribution. Additionally, CO_2 at a temperature of 10 °C is injected at Snøhvit, and heated to 95 °C by the formation, this violates the assumption of constant temperature in the analytical expression. Furthermore, CO_2 injection in the Tubåen Fm. occasionally halted due to operational challenges at the LNG plant (Hansen et al., 2012). Hence, the injection rate was not constant. However, a constant injection rate is assumed in the model, based on the total amount of CO_2 injected into Tubåen 1 during the 16 months between the seismic surveys. A rapid pressure increase was observed during autumn 2008 that was interpreted to be caused by precipitated salt (Hansen et al., 2012). Based on the pressure increase it is nearby to assume that evaporation of the residual brine occurs at an early stage of injection, and violate the assumption of an uniform CO_2 saturation within the plume. A mixture of methyl ethyl glycol (MEG) and water was injected weekly into the formation to remove the precipitated salt (Hansen et al., 2012). The injected MEG may have reduced the CO_2 saturation and hence dimmed the fluid effect on the time-lapse seismic data. Despite all the deviation from the assumptions made in the analytical expression, there is a good agreement in the shape of the CO_2 layer radius found from the analytical solution and the time-lapse seismic measurements.

The result of White et al. (2014) shows that the pore pressure response spreads more widely through the reservoir. The assumption of pressure communication is supported by Hansen et al. (2011) who found that a thicker part of the Tubåen Fm. had to be pressurized, or that the pressure sensitivity was higher than the rock physics predicted, to explain the size of the time-shift through the Tubåen Fm. There are no indications of pressure communication from the time-lapse seismic data (Fig. 2), yet this could be explained by the seismic resolution.

The viscosity ratio between brine and CO_2 is approximately 8 under the pressure and temperature regimes of the Tubåen Fm. The CO_2 is less viscous than the brine, and hence has the highest mobility. Based on this significant viscous fingering effects are expected to occur and the effective CO_2 saturation of the formation is low. The viscous fingers are most likely below the resolution of the seismic data, and are difficult to detect.

7. Conclusion

The distribution and saturation of CO_2 in the Tubåen 1 sandstone unit have been estimated from an analytical expression and two time-lapse seismic methods. The analytical expression assumes that capillary pressure can be ignored, and that the fluid flow is viscous dominated. Furthermore, it supposes the CO_2 distribution inside the plume is uniform and equal to $1 - S_{br} = 0.87$, whilst the reduction in effective CO_2 saturation is due to the thinning of the layer. The influence of gravity has been shown to be ignorable on the reservoir CO_2 flow. Analytical results suggest CO_2 fills the entire sandstone unit up to approximately 50 m away from the injection well before the plume is reduced to a thin wedge that propagates along the top of the formation. The maximum radius of the CO_2 layer from the analytic expression is 750 m, with 400 m likely to be observable above the time-lapse noise level.

The spatial extent of the CO_2 plume obtained from time-lapse spectral decomposition and inverted from time-lapse AVO seismic data is in good agreement. The CO_2 is limited to an area close to the injection well, with an elongated shape in the channel direction. From the time-lapse spectral decomposition one finds that the injected CO_2 migrates as a thin layer in the Tubåen 1 sandstone unit, whereas the pore pressure response spreads more widely through the reservoir. The reduction in CO_2 saturation away from the injection well is expected to be a reduction in effective CO_2 saturation within the sandstone unit, as the negligible capillary pressure will lead to a constant saturation within the plume. The revised approach presented in this study demonstrated that no conclusions about the CO_2 saturation within the plume can be drawn from the AVO inverted saturation, besides that the saturation is between 0.4 and 0.87.

A good match can be found between the CO_2 layer thickness and effective CO_2 saturation in the sandstone unit by scaling the CO_2 saturation inverted from seismic according to the analytical expression. The good match is an indication of viscous dominated CO_2 flow and that the CO_2 saturation within the layer is close to the residual brine saturation. The maximum observable CO_2 layer radius inverted from time-lapse seismic is on average 405 m in the channel direction, and 273 m perpendicular to the channel direction.

Acknowledgements

We thank Statoil and their partners Petoro, Total E&P Norge, GDF SUEZ E&P Norge, and RWE Dea Norge AS for permission to use their data. Bård Osdal at Statoil is acknowledged for providing the data and information regarding the Snøhvit field. This publication has been produced with support from the BIGCCS Centre, performed under the Norwegian research programme Centres for Environment-friendly Energy Research (FME). The authors acknowledge the following partners for their contributions: Aker Solutions, ConocoPhillips, Gassco, Shell, Statoil, TOTAL, GDF SUEZ and the Research Council of Norway (193816/S60). Martin Landrø acknowledges the financial support from the Norwegian Research Council to the ROSE consortium at NTNU. Jim White publishes with permission of the Executive Director, British Geological Survey (NERC). Jon Kleppe is acknowledged for help and discussions regarding reservoir fluid flow. We are highly grateful for the code to estimate the shape of the CO_2-brine interface given by Jan M. Nordbotten.

References

Arts, R., Eiken, O., Chadwick, A., Zweigel, P., Meer, L.V.D., Zinszner, B., 2004. Monitoring of CO_2 injected at Sleipner using time-lapse seismic data. Energy 29, 9.

Bachu, S., Bonijoly, D., Bradshaw, J., Burruss, R., Holloway, S., Christensen, N.P., Mathiassen, O.M., 2007. CO_2 storage capacity estimation: methodology and gaps. Int. J. Greenh. Gas Control 1, 430–443.

Batzle, M., Wang, Z., 1992. Seismic properties of pore fluids. Geophysics 57, 1396–1408.

Bennion, D.B., Bachu, S., 2008. Drainage and imbibition relative permeability relationships for supercritical CO_2/brine and H_2S/brine systems in intergranular sandstone, carbonate, shale, and anhydrite rocks. SPE Reserv. Evaluat. Eng. 11, 487–496.

Brie, A., Pampuri, F., Marsala, A.F., Meazza, O., 1995. Shear sonic interpretation in gas-bearing sands. In: SPE 30595, pp. 701–710.

Bryant, S.L., Lakshminarasimhan, S., Pope, G.A., 2008. Buoyancy-dominated multiphase flow and its effect on geological sequestration of CO_2. SPE J. 13, 447–454.
Cavanagh, A., 2013. Benchmark calibration and prediction of the Sleipner CO_2 plume from 2006 to 2012. Energy Procedia 37, 3529–3545.
Chadwick, A., Arts, R., Eiken, O., Williamson, P., Williams, G., 2006. Geophysical monitoring of the CO_2 plume at Sleipner, North Sea. In: Lombardi, S., Altunina, L.K., Beaubien, S.E. (Eds.), Advances in the Geological Storage of Carbon Dioxide. Springer, Netherlands.
Chadwick, A., Williams, G., Delepine, N., Clochard, V., Labat, K., Sturton, S., Buddensiek, M., Dillen, M., Nickel, M., Lima, A., Arts, R., Neele, F., Rossi, G., 2010. Quantitative analysis of time-lapse seismic monitoring data at the Sleipner storage operation. The Leading Edge 29, 170–177.
Class, H., Ebigbo, A., Helmig, R., Dahle, H., Nordbotten, J., Celia, M., Audigane, P., Darcis, M., Ennis-King, J., Fan, Y., Flemisch, B., Gasda, S., Jin, M., Krug, S., Labregere, D., Naderi Beni, A., Pawar, R., Sbai, A., Thomas, S., Trenty, L., Wei, L., 2009. A benchmark study on problems related to CO_2 storage in geologic formations. Comput. Geosci. 13, 409–434.
Eiken, O., Ringrose, P., Hermanrud, C., Nazarian, B., Torp, T.A., Høier, L., 2011. Lessons learned from 14 years of CCS operations: Sleipner in Salah and Snøhvit. Energy Procedia 4, 5541–5548.
Gassmann, F., 1951. Uber die Elastizitat poroser Medien. Vierteljahrsschrift der Naturforschenden Gesselschaft 96, 1–23.
Grude, S., Landrø, M., Dvorkin, J., 2014. Pressure effects caused by CO_2 injection in the Tubåen formation, the Snøhvit field. Int. J. Greenh. Gas Control 27, 178–187.
Grude, S., Landrø, M., Osdal, B., 2013. Time-lapse pressure–saturation discrimination for CO_2 storage at the Snøhvit field. Int. J. Greenh. Gas Control 19, 369–378.
Hansen, O., Eiken, O., Østmo, S., Johansen, R.I., Smith, A., 2011. Monitoring CO_2 injection into a fluvial brine-filled sandstone formation at the Snøhvit field, Barents Sea. In: SEG Technical Program Expanded Abstracts.
Hansen, O., Gilding, D., Nazarian, B., Osdal, B., Ringrose, P., Kristoffersen, J.-B., Eiken, O., Hansen, H., 2012. Snøhvit: the history of injecting and storing 1 Mt CO_2 in the fluvial Tubåen Fm, GHGT-11. In: Kyoto International Conference Center, Japan.
Hansen, O., Gilding, D., Nazarian, B., Osdal, B., Ringrose, P., Kristoffersen, J.-B., Eiken, O., Hansen, H., 2013. Snøhvit: the history of injecting and storing 1 Mt CO_2 in the Fluvial Tubåen Fm. Energy Procedia 37, 3565–3573.
IPCC, 2005. Carbon Dioxide Capture and Storage: Special report of the Intergovernmental Panel on Climate Change. Cambridge University Press, New York.
Ivanova, A., Kashubin, A., Juhojuntti, N., Kummerow, J., Henninges, J., Juhlin, C., Lüth, S., Ivandic, M., 2012. Monitoring and volumetric estimation of injected CO_2 using 4D seismic, petrophysical data, core measurements and well logging: a case study at Ketzin, Germany. Geophys. Prospect. 2012, 16.
Juhlin, C., Young, R., 1993. Implications of thin layers for amplitude variation with offset (AVO) studies. Geophysics 58, 1200–1204.
Kestin, J., Khalifa, H.E., Abe, Y., Grimes, C.E., Sookiazian, H., Wakeham, W.A., 1978. Effect of pressure on the viscosity of aqueous sodium chloride solutions in the temperature range 20–150°C. J. Chem. Eng. Data 23, 328–336.
Landrø, M., 2001. Discrimination between pressure and fluid saturation changes from time-lapse seismic data. Geophysics 66, 836–844.
Laughlin, K., Garossino, P., Partyka, G., 2002. Spectral Decomposition Applied to 3-D. Geophysical Corner, AAPG Explorer, pp. 28–31.
Lin, T.L., Phair, R., 1993. AVO tuning. In: SEG Technical Program Expanded Abstracts.
Lindeberg, E., Wessel-Berg, D., 1997. Vertical convection in an aquifer column under a gas cap of CO_2. Energy Convers. Manag. 38 (Suppl.), S229–S234.
Møll Nilsen, H., Herrera, P.A., Ashraf, M., Ligaarden, I., Iding, M., Hermanrud, C., Lie, K.-A., Nordbotten, J.M., Dahle, H.K., Keilegavlen, E., 2011. Field-case simulation of CO_2-plume migration using vertical-equilibrium models. Energy Procedia 4, 3801–3808.
Nakatsuka, Y., Kim, J., Xue, Z., Matsuoka, T., Kubota, K.,2009. Quantitative estimation of CO_2 saturation in saline aquifer storage based on resistivity data. In: Proceedings of the 9th SEGJ International Symposium. Sapporo, Japan.
Nordbotten, J., Celia, M., Bachu, S., 2005. Injection andstorage of CO_2 in deep saline aquifers: analytical solution for CO_2 plume evolution during injection. Transport Porous Media 58, 339–360.
Nordbotten, J.M., Celia, M.A., 2006. Similarity solutions for fluid injection into confined aquifers. J. Fluid Mech. 561, 20.
Okwen, R.T., Stewart, M.T., Cunningham, J.A., 2010. Analytical solution for estimating storage efficiency of geologic sequestration of CO_2. Int. J. Greenh. Gas Control 4, 102–107.
Osdal, B., Zadeh, H.M., Johansen, S., Gilding, D.,2013. CO_2 saturation and thickness prediction from 4D seismic data at Snøhvit field. In: 75th EAGE Conference and Exhibition incorporating SPE EUROPEC 2013. London, UK.
Polak, S., Cinar, Y., Holt, T., Torsæter, O., 2011. An experimental investigation of the balance between capillary, viscous, and gravitational forces during CO_2 injection into saline aquifers. Energy Procedia 4, 4395–4402.
Reuss, A., 1929. Berechnung der Fließgrenze von Mischkristallen auf Grund der Plastizitätsbedingung für Einkristalle. J. Appl. Math. Mech. 9, 49–58.
Scalabrin, G., Marchi, P., Finezzo, F., Span, R., 2006. A reference multiparameter thermal conductivity equation for carbon dioxide with an optimized functional form. J. Phys. Chem. Ref. Data 35, 1549–1575.
Sengupta, M., (Ph.D. thesis) 2000. Integrating Rock Physics and Flow Simulation to Reduce Uncertainties in Seismic Reservoir Monitoring. Stanford University.
Span, R., Wagner, W., 1996. A new equation of state for carbon dioxide covering the fluid region from the triple-point temperature to 1100 K at pressures up to 800 MPa. J. Phys. Chem. Ref. Data 25, 1509–1596.
Taku IDE, S., Jessen, K., Orr Jr., F.M., 2007. Storage of CO_2 in saline aquifers: effects of gravity, viscous, and capillary forces on amount and timing of trapping. Int. J. Greenh. Gas Control 1, 481–491.
Voigt, W., 1887. Theoretische Studien über die Elasticitätsverhältnisse der Krystalle. Abhandlungen der Königlichen Gesellschaft der Wissenschaften in Goöttingen 34, 3–51.
White, J.C., Williams, G.A., Grude, S., Chadwick, A.,2014. Utilising spectral decomposition to determine the distribution of injected CO_2 at the Snøhvit field. In: Fourth EAGE CO_2 geological storage workshop demonstrating storage integrity and building confidence in CCS 22–24 April. Stavanger, Norway.
Widess, M., 1973. How thin is a thin BED? Geophysics 38, 1176–1180.
Williams, G., Chadwick, A., 2012. Quantitative seismic analysis of a thin layer of in the Sleipner injection plume. Geophysics 77, R245–R256.